View metadata, citation and similar papers at core.ac.uk

brought to you by CORE

provided by UNH Scholars' Repository

University of New Hampshire
University of New Hampshire Scholars' Repository

Earth Sciences Scholarship | Earth Sciences

8-27-2007

Impact of multiscale dynamical processes and mixing on the chemical composition of the upper troposphere and lower stratosphere during the Intercontinental Chemical Transport Experiment–North America

T D. Fairlie
Harvard University

Melody A. Avery
NASA

R B. Pierce
NOAA

J Al-Saadi
NASA

Jack E. Dibb
University of New Hampshire, jack.dibb@unh.edu

Recommended Citation

Fairlie, T. D., M. A. Avery, R. B. Pierce, J. Al-Saadi, J. Dibb, and G. Sachse (2007), Impact of multiscale dynamical processes and mixing on the chemical composition of the upper troposphere and lower stratosphere during the Intercontinental Chemical Transport Experiment–North America, J. Geophys. Res., 112, D16S90, doi:10.1029/2006JD007923.

This Article is brought to you for free and open access by the Earth Sciences at University of New Hampshire Scholars' Repository. It has been accepted for inclusion in Earth Sciences Scholarship by an authorized administrator of University of New Hampshire Scholars' Repository. For more information, please contact nicole.hentz@unh.edu.

See next page for additional authors

Follow this and additional works at: https://scholars.unh.edu/earthsci_facpub

 Part of the Atmospheric Sciences Commons

Authors
T D. Fairlie, Melody A. Avery, R B. Pierce, J Al-Saadi, Jack E. Dibb, and G W. Sachse

This article is available at University of New Hampshire Scholars' Repository: https://scholars.unh.edu/earthsci_facpub/123

Impact of multiscale dynamical processes and mixing on the chemical composition of the upper troposphere and lower stratosphere during the Intercontinental Chemical Transport Experiment–North America

T. Duncan Fairlie,[1] Melody A. Avery,[1] R. Bradley Pierce,[1] Jassim Al-Saadi,[1] Jack Dibb,[2] and Glen Sachse[1]

Received 15 August 2006; revised 24 April 2007; accepted 30 May 2007; published 21 August 2007.

[1] We use high-frequency in situ observations made from the DC8 to examine fine-scale tracer structure and correlations observed in the upper troposphere and lower stratosphere during INTEX-NA. Two flights of the NASA DC-8 are compared and contrasted. Chemical data from the DC-8 flight on 18 July show evidence for interleaving and mixing of polluted and stratospheric air masses in the vicinity of the subtropical jet in the upper troposphere, while on 2 August the DC-8 flew through a polluted upper troposphere and a lowermost stratosphere that showed evidence of an intrusion of polluted air. We compare data from both flights with RAQMS 3-D global meteorological and chemical model fields to establish dynamical context and to diagnose processes regulating the degree of mixing on each day. We also use trajectory mapping of the model fields to show that filamentary structure due to upstream strain deformation contributes to tracer variability observed in the upper troposphere. An Eulerian measure of strain versus rotation in the large-scale flow is found useful in predicting filamentary structure in the vicinity of the jet. Higher-frequency (6–24 km) tracer variability is attributed to buoyancy wave oscillations in the vicinity of the jet, whose turbulent dissipation leads to efficient mixing across tracer gradients.

Citation: Fairlie, T. D., M. A. Avery, R. B. Pierce, J. Al-Saadi, J. Dibb, and G. Sachse (2007), Impact of multiscale dynamical processes and mixing on the chemical composition of the upper troposphere and lower stratosphere during the Intercontinental Chemical Transport Experiment–North America, *J. Geophys. Res.*, *112*, D16S90, doi:10.1029/2006JD007923.

1. Introduction

[2] During the summer of 2004 the NASA DC-8, carrying a comprehensive chemical sensor payload, participated in a major aircraft field campaign making measurements over North America in the troposphere and lowermost stratosphere. The Intercontinental Chemical Transport Experiment–North America (INTEX-NA) was designed to understand the transport and transformation of gases and aerosols on transcontinental/intercontinental scales, and their impact on air quality and climate [*Singh et al.*, 2006]. Particular goals of INTEX-NA were to characterize fluxes of ozone and its precursors to and from the North American continent, and to provide correlative measurements to validate observations from satellites. The INTEX-NA measurements were a critical part of a much larger, multiagency effort, ICARTT, described by *Fehsenfeld et al.* [2006]. Together, measurements and modeling efforts associated with INTEX-NA and ICARTT provide a rich data set from airborne and ground-based remote sensors, sonde and aircraft-based in situ instrumentation, and modeled chemical fields, spanning a wide range of temporal resolution and spatial scales.

[3] A fundamental issue in Earth science is to quantify the human impact on the climate and composition of the earth's atmosphere. Much effort has been focused on quantifying the impact of anthropogenic emissions of photochemically active gases and aerosols on air quality, the oxidizing capacity of the atmosphere [*Logan et al.*, 1981; *Chameides and Davis*, 1982], and climate [*Fishman et al.*, 1979; *Jacob and Gilliland*, 2005, and references therein]. There has also been much effort to distinguish the impact of ozone produced via pollution in the troposphere from that originating in the stratosphere [e.g., *Fishman and Crutzen*, 1978; *Liu et al.*, 1980; *Shapiro*, 1980; *Wang et al.*, 1998; *Logan*, 1985]. Much of the difficulty in pursuing this latter objective is that transport processes, responsible for redistributing ozone and its precursors in the atmosphere, operate on a wide range of spatial and temporal scales, from planetary-scale motions that move material quasi-isentropically to small-scale intermittent processes like convection and turbulence that can redistribute material across isentropes. This presents a serious challenge for global- and regional-scale models that are used to make such quantitative assessments. The models can capture transport processes at grid and higher scales, but subgrid-scale and intermittent

[1]NASA Langley Research Center, Hampton, Virginia, USA.
[2]College of Engineering and Physical Sciences, University of New Hampshire, Durham, New Hampshire, USA.

Copyright 2007 by the American Geophysical Union.
0148-0227/07/2006JD007923

processes like convection must be parameterized, so that the full range of upscale energy transfer is not represented [*Tuck et al.*, 2004, 2005]. Because laminae of air influenced both by the stratospheric and tropospheric pollution are commonly observed in the upper troposphere, it is often difficult to differentiate ozone structure of natural from anthropogenic origin.

[4] The upper troposphere and lowermost stratosphere, that region of the stratosphere below potential temperatures of around 380 K whose isentropes span the tropopause [*Holton et al.*, 1995], are critical regions for assessing the human impact on radiatively active trace gases such as ozone, because radiative forcing due to changes in such gases is most sensitive in this region [*Forster and Shine*, 1997]. Of particular interest is the region around upper tropospheric jet streams. These jets are typically characterized by strong horizontal and vertical wind shears, thermal gradients, and associated cross-jet gradients in potential vorticity and chemical constituents, which provide a natural separation between the troposphere and the lowermost stratosphere [*Shapiro*, 1980]. Transport along a jet can be very rapid so that anthropogenic pollution lofted from below can have a significant long-range (intercontinental) component and diverse origins. Jets support a wide range of spatial and temporal scales of motion, from inertial (Rossby) waves, which propagate upon lateral gradients in potential vorticity, to buoyancy waves, and turbulence driven by vertical wind shear. Strong accelerations in the vicinity of jet streaks and strong curvature associated with Rossby wave deformation can lead to tropopause folding, interweaving (filamentation) of stratospheric and tropospheric air masses, and intermediate-scale horizontal tracer variability in quasi-conserved chemical species like ozone [e.g., *Shapiro*, 1980; *Appenzeller et al.*, 1996] via stretching of tracer gradients along streamlines. Moreover, convective and prefrontal (warm conveyor belt) lifting during cyclogenesis can bring boundary layer pollutants into close proximity with stratospherically influenced air subsiding in dry tongues behind upper frontal systems [*Cooper et al.*, 2004; *Esler et al.*, 2003]. Smaller-scale inertio-gravity or high-frequency gravity waves can perturb the alignment of isentropic surfaces where tracer gradients are large [*Danielsen et al.*, 1991; *Chan et al.*, 1991], and wind-shear-driven turbulence in tropopause folds results in irreversible mixing of chemical characteristics across air mass interfaces [*Shapiro*, 1980; *Cho et al.*, 1999].

[5] Thus the generation of mesoscale tracer structure in the vicinity of upper tropospheric jets and boundaries between polluted and stratospheric air masses can have important consequences for exchange of air across the tropopause and the irreversible mixing of polluted and stratospheric air masses, and introduces significant complexity for validating satellite measurements [*Sparling et al.*, 2006]. Understanding and quantifying irreversible material exchange across the tropopause, and mixing of air of differing origins in that region is a goal of the broader scientific community, including that of INTEX-NA. The objective in this paper is to provide improved characterization of the impact of planetary to mesoscale dynamical and transport processes on the chemical composition of the upper troposphere and lowermost stratosphere during INTEX-NA, and to differentiate the effects of planetary-scale motions from smaller-scale buoyant and turbulent motions. We use high-frequency (1 s) aircraft in situ chemical observations made from the DC8 to characterize mesoscale tracer structure, and use constituent correlations to distinguish air of different origins. We use a global 3-D model, RAQMS [*Pierce et al.*, 2003], to provide dynamical context and insight into larger-scale transport processes to aid interpretation of the observational data. We apply a trajectory mapping technique (reverse domain filling, or RDF) to the global model fields to help assess the extent to which upstream strain deformation of tracer gradients contributes to mesoscale variability observed in the tracer fields, and use a measure of large-scale strain versus rotation, Q [*Haynes*, 1990], to identify regions where filamentation is expected to occur. Questions posed in this study include: To what extent can trajectory mapping be used to explain some of the mesoscale tracer variability observed from the DC8? Can the Q field provide useful information on the preferred locations where small-scale tracer structure is found?

[6] To answer these questions we compare and contrast two flights of the DC-8 during the INTEX-NA deployment to Pease, New Hampshire. The two flights occurred over a similar geographical region of New England, Eastern Canada and the western Atlantic. The DC-8 sampled the upper troposphere in the vicinity of the subtropical jet on both flights. Measurements of carbon monoxide (CO), hydrogen cyanide (HCN) and reactive nitrogen species (NOy), suggest that the upper troposphere was significantly polluted [*Singh et al.*, 2007], while tracer correlations and ozone soundings show that the upper troposphere was significantly stratospherically influenced (see Figure 2 in section 3) [*Thompson et al.*, 2007]. However, the two flights were found to have a contrasting degree of tracer variability, differing pollution sources, and observations show varying amounts of mixing between stratospheric and tropospheric air. We use the RAQMS model to examine differences in the meteorological context and chemical transport environment of the flights, and in situ chemical and dynamical variables to interpret the observed structure and processes at work.

2. Tools/Methods

2.1. In Situ Measurements and Merged Data

[7] The NASA DC-8 contained a full payload of instruments measuring photochemically active tracers during INTEX-NA [*Singh et al.*, 2006]. In this paper we focus on the in situ measurements of ozone, carbon monoxide, nitric acid and total peroxynitrates (TPNs). The in situ ozone and carbon monoxide measurements were made at 1 s temporal resolution by nitric oxide chemiluminesence [*Avery et al.*, 2001; M. A. Avery et al., FASTOZ: An accurate, fast-response in situ ozone measurement system for aircraft campaigns, submitted to *Journal of Oceanic and Atmospheric Technologies*, 2006] and by diode laser spectrometer [*Sachse et al.*, 1987]. Both instruments have demonstrated a 2–3 Hz response time in the lab, and show anticorrelation at 1 s in stratospheric air that would not be possible from random noise, however a formal scaling analysis has not yet been performed for these measurements. TPNs were measured by thermal dissociation and laser induced fluorescence, with a data collection cycle of

25 s [*Thornton et al.*, 1999], and include both PAN and pernitric acid, HNO4. Nitric acid was measured by mist chamber collection at 100 s [*Dibb et al.*, 2006]. Two merged chemical and navigational data sets were created, one at 1 s to correlate the fast data streams, and the other at 100 s, corresponding to the nitric acid sampling time. The 1 s merged data stream includes a 2 s lag of the navigational and CO data behind the ozone data, which was calculated from the correlations using a similar method to *Murphy* [1989]. All reported TPN data and the fast-response data were averaged over the longer nitric acid measurement cycle for inclusion in the slower merged data stream.

2.2. RAQMS Model Description

[8] The 3-D model used in this study is the LaRC/UW Realtime Air Quality Modeling System (RAQMS) [*Pierce et al.*, 2007]. RAQMS is a portable, global- to regional-scale meteorological and chemical modeling system which has been developed for assimilating remote observations of atmospheric chemical composition and predicting air quality globally or regionally [*Pierce et al.*, 2002]. RAQMS ozone fields are constrained via assimilation of satellite ozone column and profile measurements. This study uses a global simulation conducted for the INTEX-NA period. The model uses a hybrid (sigma-theta) coordinate in the vertical. The simulation was conducted at a horizontal resolution of 1.4° by 1.4°, with 35 layers, spanning the troposphere and stratosphere. Vertical resolution near the tropopause depends on the vertical gradient in potential temperature and varies between ~200 m and 1 km. *Pierce et al.* [2007] present an evaluation of the RAQMS simulation and an analysis of the continental US O3 and NOy budgets. J. Al-Saadi et al. (A Lagrangian characterization of the sources and chemical transformation of air influencing the US and Europe during the 2004 ICARTT/INTEX-NA campaign, manuscript in preparation, hereinafter referred to as A-S06) use trajectory mapping to identify the dominant contributions to O3 distributions over the INTEX domain and Europe, and their air mass origins. The global component of RAQMS has at its dynamical core the University if Wisconsin (UW) global hybrid model [*Zapotocny et al.*, 1991, 1994]. The RAQMS unified stratosphere/troposphere chemistry module has been developed to represent photochemical processes governing ozone formation and destruction within Earth's atmosphere from the surface to about 60 km. Full details the chemical formulation are given by *Pierce et al.* [2007].

2.3. Langley Trajectory Model (LTM)

[9] Three-dimensional trajectory calculations are conducted using a new version of the Langley trajectory model (LTM) [*Pierce and Fairlie*, 1993; *Pierce et al.*, 1994] that has been configured to use RAQMS hybrid coordinate wind fields. The LTM has been used to explore small-scale tracer variability and filamentation due to large-scale flow fields in the stratosphere [*Pierce et al.*, 1994; *Fairlie et al.*, 1997], and has been used to characterize sources and chemical transformations during INTEX-A (A-S06). It is currently used as the trajectory component of the Infusing Satellite Data into Environmental Applications (IDEA) program to provide real-time PM2.5 air quality forecast guidance [*Al-Saadi et al.*, 2005].

[10] In this study, the LTM is used to construct reverse-domain-filled (RDF) ozone fields along aircraft flight tracks to compare with the measured in situ ozone data. The LTM samples global chemical and dynamical fields from the RAQMS model. RDF is a trajectory mapping technique that has shown potential to represent coarsely resolved constituent fields at higher resolution, with higher information content, than originally observed [*Sutton et al.*, 1994] (or modeled). RDF is assumed to simulate the cascade of tracer variability to small scales due to large-scale differential advection. RDF has been used to explain the development of small-scale tracer structure in the stratosphere [*Fairlie et al.*, 1997]. *Beuermann et al.* [2002] used RDF to interpret small-scale ozone and specific humidity structure observed in the vicinity of the polar jet during the STREAM campaign. Here, we use RDF to assess how much tracer variability observed along aircraft flight tracks during INTEX can be explained by large-scale dynamical processes (such as Rossby wave-breaking) and intermittent diabatic processes captured within the RAQMS modeling system. *Fairlie et al.* [1997] cautioned that RDF does not generally show skill in adding small-scale information when applied to fields of highly derived quantities, e.g., PV, but can provide useful information when it refines structure that already exists in conventional analyses. Its application to dynamically and chemically consistent ozone analyses from RAQMS is expected to be more fruitful. RDF is not expected to add quantitative information on tracer variability that arises from small-scale dynamical processes that are not explicitly represented in RAQMS, e.g., gravity waves, nor from small-scale nonconservative processes neglected by the trajectory calculations, e.g., turbulent mixing.

2.4. Mixing Diagnostic

[11] We also use a measure of the relative contribution of strain and rotation in the large-scale flow, Q, to explore whether such a diagnostic can be used as an objective synoptic-scale predictor of intermediate to small-scale ozone variability in the upper troposphere. Q is defined by $2Q = D{:}D - W{:}W$, where D is the rate of deformation tensor, $D = \frac{1}{2}(v\overleftarrow{\nabla} + \overrightarrow{\nabla}v)$ and W is the vorticity or spin tensor $W = \frac{1}{2}(v\overleftarrow{\nabla} - \overrightarrow{\nabla}v)$. For quasi-horizontal 2-D atmospheric flow Q, normalized by the Earth's rotation, is given by

$$Q = \frac{1}{2}\left(\frac{1}{\cos\phi}\frac{\partial u}{\partial \lambda} - v\tan\phi\right)^2 + \frac{1}{2}\left(\frac{\partial v}{\partial \phi}\right)^2 + \frac{\partial u}{\partial \phi}\left(\frac{1}{\cos\phi}\frac{\partial v}{\partial \lambda} + u\tan\phi\right)^2, \quad (1)$$

where λ and ϕ are longitude and latitude respectively [*Haynes*, 1990]. Q provides a measure of the relative importance of strain and rotation on fluid elements in an Eulerian reference frame. For positive Q, strain predominates and fluid elements are stretched, with line elements expected to increase at a rate $\exp(Q^{1/2}\, t)$ [*Haynes*, 1990], so that $Q^{1/2}$ corresponds to the local Liapunov exponent [*Ottino*, 1989]. Where Q is negative, rotation predominates, and line elements do not systematically increase in length. Positive Q is found to be associated with regions of Rossby wave breaking, where efficient stirring of air masses occurs,

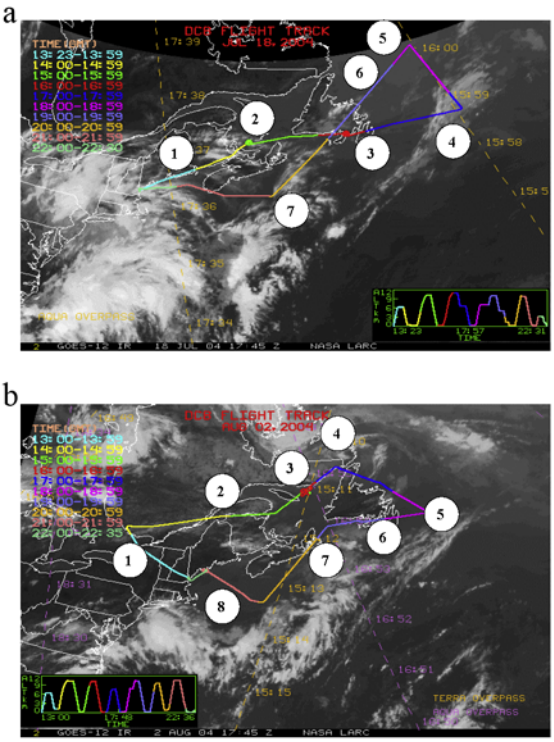

Figure 1. NOAA GOES 12 IR water vapor image for 1745 UT on (a) 18 July and (b) 2 August with overlaid DC8 flight tracks. Altitude profiles for the flights are inset. Level flight legs are numbered 1–7 and 1–8 respectively for each of the two flights. (Courtesy D. Westberg, SAIC.)

while negative Q is associated with closed circulations [*Haynes*, 1990; *Fairlie et al.*, 1999]. Efficient stirring promotes irreversible mixing by increasing interfacial area between distinct air masses [*Aref and Balachander*, 1986]. Q has been used as a measure the mixing efficiency of trace gases on isentropic surfaces in regions of strong gradients and planetary wave breaking [*Fairlie et al.*, 1999; *Pierce et al.*, 2003]. Here, we compute time-averaged Q following air parcel back trajectories as a measure of the deformation history of the parcels, and explore whether this quantity can predict small-scale tracer variability observed in the upper troposphere during INTEX-A. For positive Q we anticipate a history of shear strain leading to filamentation, tight gradients, and mixing.

3. Comparison of Upper Tropospheric in Situ Observations on 18 July and 2 August

[12] In this section, we compare and contrast chemical tracer variability and correlations observed on two flights during INTEX-A, those of 18 July and 2 August. The two flights were selected because they took place over a similar geographical region of New England, Eastern Canada, and the Atlantic seaboard, yet the DC-8 measurements indicate significant differences in composition and structure in the upper troposphere.

[13] Figure 1 shows GOES 12 IR water vapor images for 1745 UT for both flight days. The flight tracks are superimposed and the vertical flight profiles are inset (images courtesy of D. Westberg, SAIC). On 18 July, there was a deep trough over the eastern U.S., with a developing low-pressure system centered over the Carolinas. Widespread clouds associated with the low are visible in the satellite image. The upper troposphere along the flight track was affected by a split flow, with a confluent region between the polar and subtropical jets encountered near points 3 and 6. On 2 August, a subtropical high dominated much of the area, with mostly clear skies and subsiding air. Unlike 18 July the subtropical jet did not extend deep into the southeast United States but was more zonally oriented near the Canadian border. As a result, except for the most northern part of the flight, the DC-8 remained on the equator side of the jet, whereas on 18 July the flight track took place primarily on the poleward side of the jet. The DC8 flight track included several level flight legs (FLs) in the upper troposphere on each day. We have numbered the locations of these legs in sequence on each panel for reference.

[14] Figure 2 shows time series of in situ ozone measured during each flight (left). (Time in this and subsequent figures is given in hours, UT). The ozone time series (black) are shown together with the altitude of the aircraft (orange). On 18 July the ozone data shows considerable mesoscale, high-amplitude variability for several of the upper level, constant pressure flight legs (FLs). Spectral analysis (not shown) reveals average and peak amplitudes of oscillations on timescales in the range 30 s to 10 min (6–120 km) on upper level flight legs to be typically 2 to 3 times those found on corresponding upper level flight legs on 2 August. (For example, the average amplitude at 100 s is 5 ppb on 18 July, but only 1 ppb on 2 August). This study aims to illuminate the reasons for the different intensities of small-scale O3 variability encountered on these 2 flights and the processes responsible for the mesoscale structure encountered on 18 July.

[15] Correlations between ozone and other trace gases also appear considerably different on these two days. Figure 2 shows scatterplots of CO versus O3 (Figure 2, middle) and HNO3 versus O3 (Figure 2, right) for observations made above 500 mbar on both days. Observations on FLs 3 for each day are highlighted in orange. We examine CO and HNO3 because CO is a tropospheric combustion tracer that is anticorrelated with stratospheric ozone, while HNO3 has a significant stratospheric source that is positively correlated with stratospheric ozone. To put these flights in a larger context, 2-D probability distributions (pdfs) of all observations made above 500 mbar from the DC-8 between 6 July and 7 August (except for the 2 flight days of our focus) are contoured on the correlation plots. The pdfs show the densest clustering of upper tropospheric observations during INTEX-A occurred at O3 mixing ratios of ~80 ppb, CO ~ 100 ppb and HNO3 < 300 ppt, which might be considered an upper tropospheric "background" measured during INTEX-NA.

[16] Each correlation plot shows tropospheric and stratospheric branches. Tropospheric pollution is characterized by enhanced CO and HNO3 with O3 values typically in the range 80–100 ppb. O3 mixing ratios larger than 80 ppb that are correlated with elevated CO are evidence of photochemical O3 production. Extremely high CO, (up to 600 ppbv of

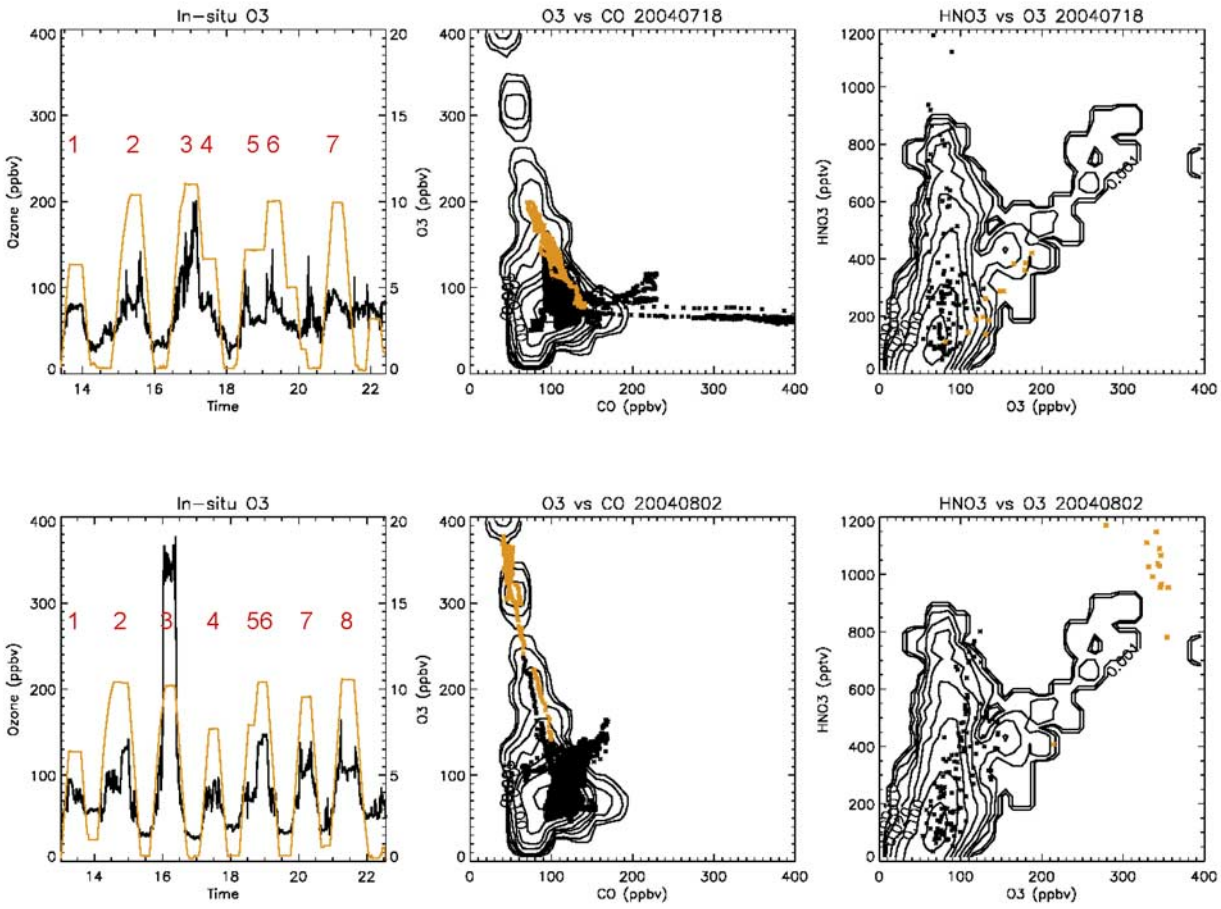

Figure 2. Time series of in situ O3 for 18 July and 2 August (black) with DC8 altitude profiles (km-ordinate on right) (orange). Scatterplots of in situ O3 versus CO and HNO3 versus O3 for points above 500 mbar for the same days, together with 2-D pdfs of all such points for remaining flights between 6 July and 10 August (contoured). Data points for FLs 3 on each day are highlighted (orange).

CO was measured), and high HNO3 observed on 18 July, with no O3 enhancement, are associated with smoke from Alaskan fires. Many of the other observations with relatively high CO and HNO3 and elevated O3 on 18 July are associated with elevated NOx and CH_2O, attributed to convective outflow. On 2 August, the majority of the measurements show O3 values enhanced above background (80 ppb) on the tropospheric branch of both scatterplots. Measurements of elevated O3, low NOx/NOy, elevated PAN/NOy, and reduced pentane to butane ratios (relative to fresh boundary layer air) in the upper troposphere during this flight are characteristic of aged pollution [*Goldstein et al.*, 2004; *Singh et al.*, 2007].

[17] The stratospheric branch of the correlation plots is characterized by a positive correlation between HNO3 and O3, with a slope of approximately 3.5 ppt:1 ppb, and a negative correlation of CO and O3, with a slope of approximately −1 ppb:4 ppb. On each of the 2 flight days, the degree of stratospheric influence encountered by the DC8 is highlighted by observations made on FL 3 (points shown in orange). On 18 July the FL3 observations are characterized by a line that connects the stratospheric and tropospheric branches on the CO-O3 correlation plot, with a slope of approximately −1 ppb:2 ppb, and intermediate values of HNO3. This "mixing line" of observations provides evidence that the DC8 encountered mixed stratospheric and polluted air masses in the upper troposphere on this day. In contrast, on 2 August the DC8 clearly sampled the lower stratosphere on FL3 with O3 values in excess of 300 ppb and CO ∼ 50 ppb. Measurements of enhanced beryllium-7 (not shown) confirm that the DC8 was flying in the stratosphere.

[18] Next we examine HNO3, ozone and PAN together and introduce results from the RAQMS model, using both tracer concentrations and correlations to compare and contrast how the observations and the model distinguish tropospheric and stratospheric air masses. PAN formation requires both NOx and hydrocarbon precursors that are most commonly associated with pollution sources. We expect PAN to be negatively correlated with stratospheric air, which lacks a hydrocarbon source. Since PAN is not particularly soluble, and has a chemical lifetime (limited by photolysis) of several months to years in the cold upper troposphere and lowermost stratosphere [*Talukdar et al.*, 1995], it is commonly used as a tracer for long-range pollution transport [e.g., *Hov et al.*, 1984], and is considered

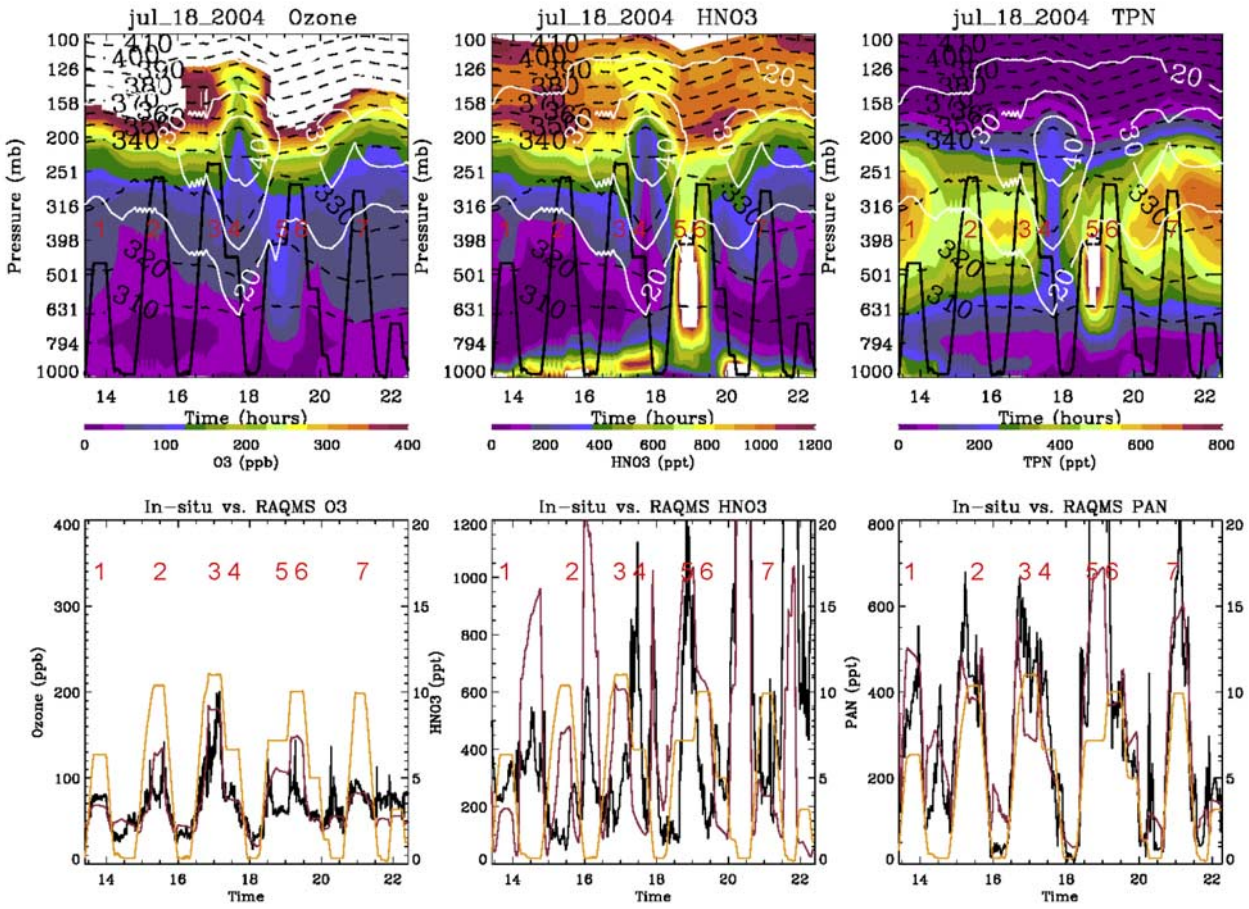

Figure 3a. (top) Curtains of RAQMS ozone, HNO3, and TPN along the DC8 flight track for 18 July 18. Isotachs (white), isentropes (black dashed) and DC8 flight profile (black) are also shown. Upper level FLs are numbered. (bottom) Corresponding time series of observed (black) and RAQMS (red) flight track data. Flight track altitude (km) is shown in orange, with axis marked at right.

an important reservoir for reactive nitrogen. In comparison, nitric acid is soluble, has a stratospheric source and is positively correlated with ozone in stratospheric air [*Dibb et al.*, 2006]. We use measured TPN, rather than PAN because the TPN measurements are available at higher frequency. The TPN measurement includes pernitric acid (HNO4); HNO4 measurements [*Kim et al.*, 2007] on the stratospheric flight legs (FLs 3) on both days ranged between 58 and 79 pptv.

[19] Figures 3a and 3b show flight curtains of ozone, HNO3 and TPN (PAN + HNO4) from the RAQMS model for the 2 flight days with the DC8 altitude profiles superimposed. Isotachs (white) and isentropes (black dashed) are also shown. Time series of the in situ observations are shown in Figures 3a and 3b (bottom) (black), with time series of RAQMS data interpolated to the flight altitude superimposed (red). As shown on the flight curtain on 18 July, the DC-8 approached the subtropical jet, shown by peak wind speeds >40 m s^{-1} and diverging isentropes, near 1750 UT from the west (poleward side) before turning to the north. Later, the DC-8 crossed the jet from north to south near 2020 UT. FLs 2, 3, and 6, which show most high-frequency variability (Figure 1), occurred on the poleward side of the jet, just beneath where RAQMS indicates large vertical ozone and HNO3 gradients marking the transition between troposphere and lower stratosphere. RAQMS shows a polluted southwesterly air stream (characterized by elevated TPN) in the mid to upper troposphere. High values of HNO3 in the boundary layer and free troposphere are characteristic of polluted air that has not been scrubbed by precipitation. Extremely high HNO3 and TPN in the RAQMS fields near 1900 UT result from simulated emissions from Alaskan fires. The DC8 sampled TPN > 500 ppt during profiling to FLs 2, 3, 6 and 7. These values were not fully captured by RAQMS, reflecting a low bias for simulated PAN in the upper troposphere and lower stratosphere. RAQMS is typically 20% high compared with observed O3 in the upper troposphere, and also shows a high bias for HNO3. These biases suggest that RAQMS underestimates convective influence and overestimates stratospheric influence [*Pierce et al.*, 2007]. Compared with the 1-s in situ data, the RAQMS analyses show limited variability on each upper level flight leg. RAQMS analyses have a resolution of 1.4° by 1.4° and thus can represent structure only on scales greater than about 150 km (~12 min flight time). TPN observations indicate that small-scale ozone variability on upper level FLs 2 and 3 is also characteristic of longer-lived tropospheric pollutants.

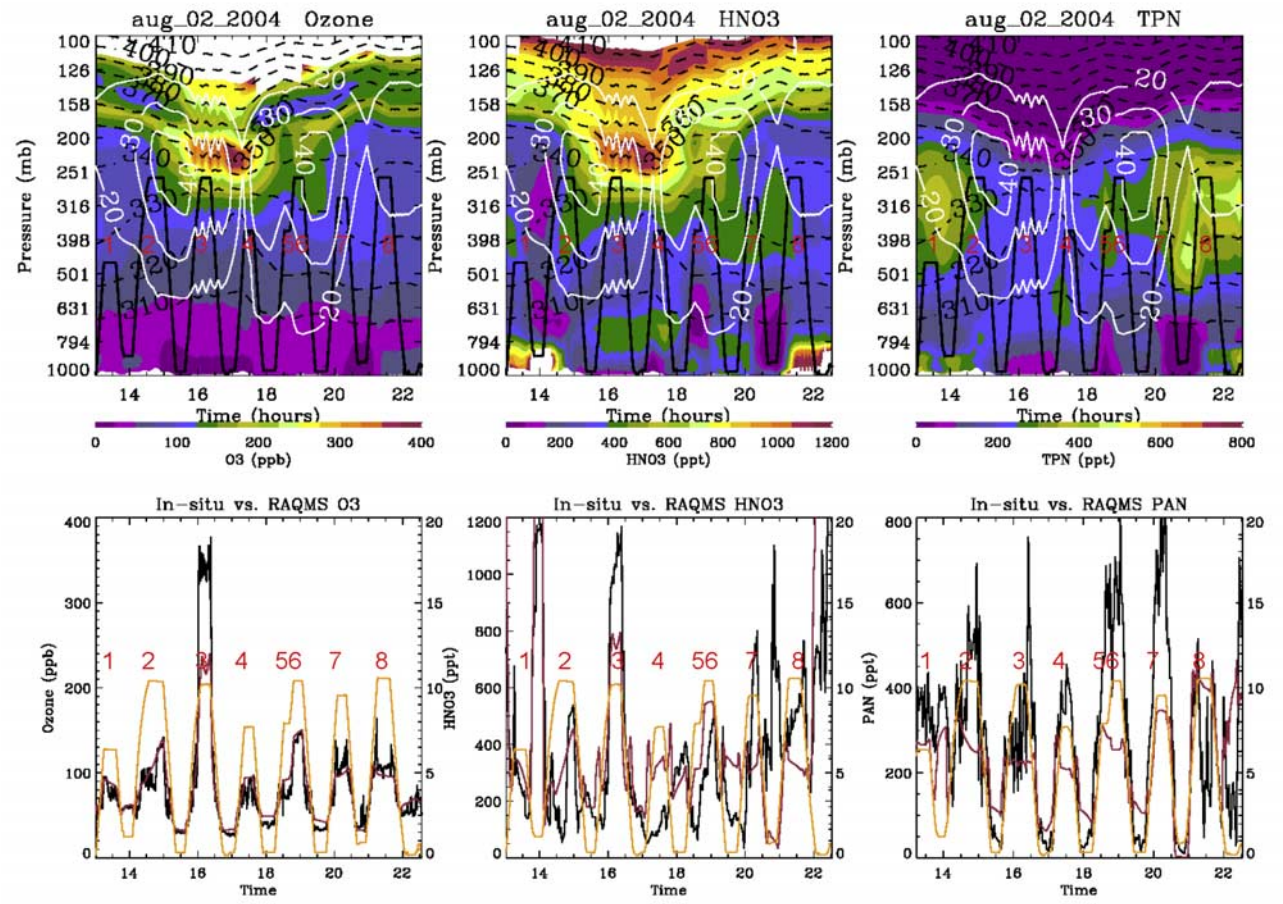

Figure 3b. As for Figure 3a but for 2 August.

[20] The flight curtain on 2 August crosses the jet from south to north near 1500 UT (~48°N) and recrosses the jet near 1930 UT. The curtains clearly show the DC8 penetrating the stratosphere, crossing steep vertical ozone and HNO3 gradients, associated with a depressed tropopause on the poleward side of the jet to reach FL3. There, O3 > 300 ppb and HNO3 > 1000 ppt were observed, together with moderate levels of O3 variability with a peak to trough range of up to 60 ppb. Very dry air with H2O around 20 ppm, and beryllium-7 values around 7000 ppt were also observed (not shown) on FL3. Of particular note, TPN in excess of 300 ppt was observed on FL3, with HNO4 concentrations of 78 ppt or below, indicating tropospheric pollution has reached the lowermost stratosphere. These observations are consistent with the deduction by *Pierce et al.* [2007] of isentropic troposphere to stratosphere fluxes at the subtropical tropopause break in the INTEX domain. FLs 2, 6 and 7, which took place equatorward of the jet core indicated a polluted air stream in the middle to upper troposphere, characterized by TPN > 500 ppt, high organics, low NOx/NOy, and elevated O3. RAQMS shows good agreement with observed O3 along the flight track, except for the stratospheric flight leg (FL 3) where both O3 and HNO3 are underpredicted. This is due to the model's underestimate of vertical constituent gradients associated with the depressed tropopause.

[21] Figure 4 shows maps of PV and O3 at 1800 UT for 18 July (330 K) and 2 August (335 K) from the RAQMS model. The DC8 flight tracks are superimposed, together with the location of selected high-altitude flights legs. Also shown are isotachs (contoured), wind vectors, and the axis of strongest winds (white line). The deep trough over the eastern U.S. on 18 July is distinguished by higher O3 and PV. The PV and O3 structure is reminiscent of "LC2" or "Type II" (cyclonic rollup) Rossby wave breaking [*Thorncroft et al.*, 1993; *Appenzeller et al.*, 1996]. In contrast, on 2 August the 335 K maps show a more zonal jet with evidence of weaker "Type I" (anticyclonic) wave breaking south of the jet with remnants of high PV and ozone drawn into the short-wave trough over the eastern U.S. and a streamer of high ozone (~120 ppb) extending southward on the east of the flight track, near 60°W. Both flight tracks span the axis of strongest winds but most of the track on 18 July (in particular FLs 2, 3, and 6) lies north of the jet core. FL3 on 18 July occurs in a region of jet confluence where isentropic descent of air parcels and tropopause folding is expected [*Shapiro*, 1981]. On 2 August, on the other hand, the flight track lies primarily south of the jet, except for FL3 which lies in the low stratosphere poleward of the jet core where the tropopause is strongly depressed.

[22] Cross sections of PV, O3, HNO3 and TPN taken along the lines A–B and C–D in Figure 4 are shown in

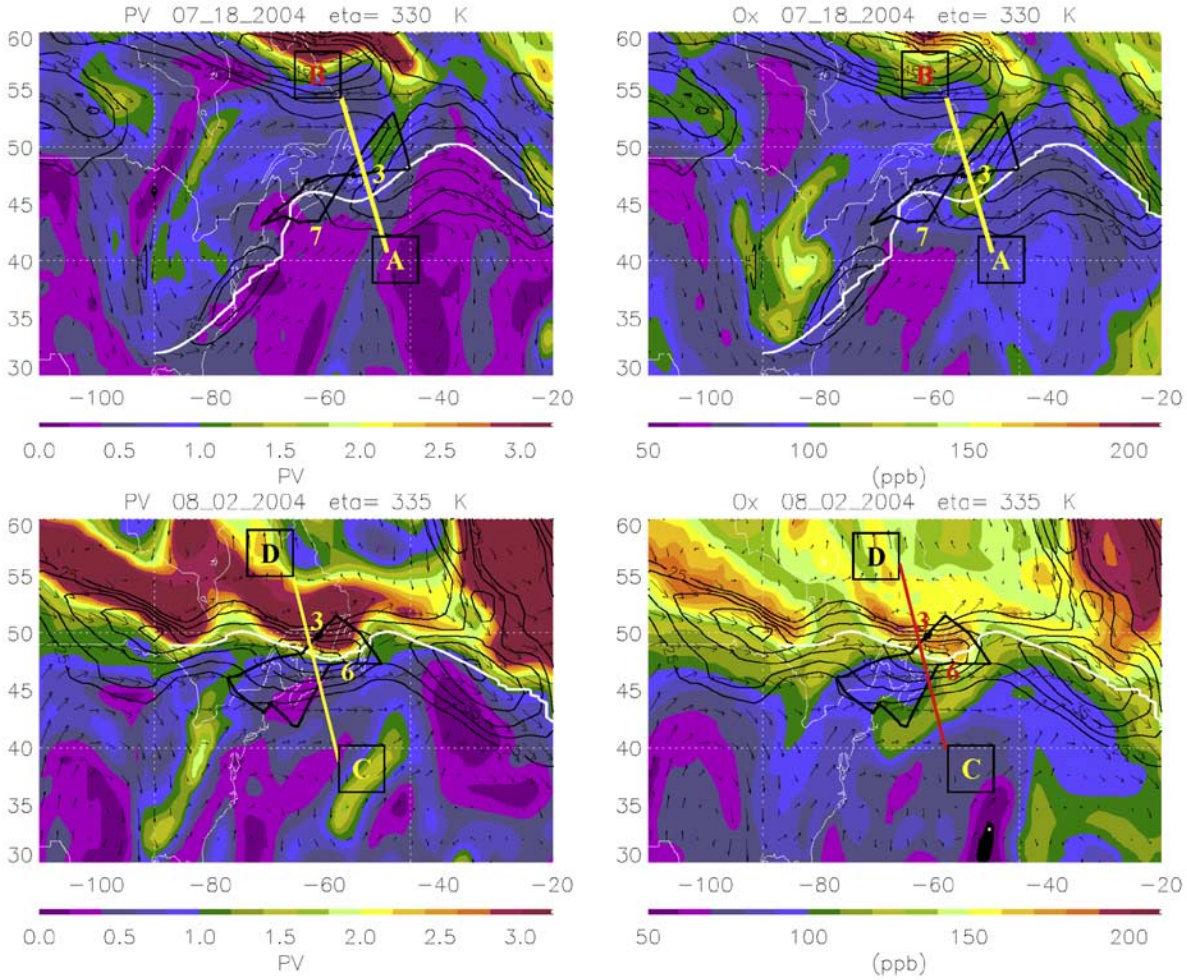

Figure 4. Maps of PV and O3 from RAQMS for 1800 UT (top) on 18 July for the 330 K eta surface and (bottom) on 2 August for the 335 K eta surface. Isotachs (black contours), wind arrows, the DC8 flight track (black), and selected flight legs are also shown. Lines A–B and C–D mark cross sections shown in Figures 5a and 5b. White lines follows the axis of strongest winds on each surface.

Figure 5. The cross sections provide a cross-jet perspective of the tracer structure in RAQMS on each of the two days and emphasize the change in tropopause elevation across the jet. Projection of the flight altitude and latitude on to the cross sections show the relative positions of the upper level flight legs on each day with respect to the jet. The cross sections for 18 July show further evidence that FLs 2, 3 and 6, characterized by enhanced mesoscale ozone variability, occurred poleward of the jet core at 45°N, just below a depressed tropopause. FL 7, which showed much less variability, occurred farther south on the equatorside of the jet. The cross sections for 2 August show the ascent of the DC8 into the low stratosphere at 48°N to FL3. There, RAQMS shows high PV, O3 and HNO3 anomalies associated with strong descent on the poleward side of the jet.

[23] The scatterplots in Figure 2 clearly indicate that the DC8 sampled mixed tropospheric and stratospheric air poleward of the jet core on 18 July. In addition, on 2 August, in situ observations of TPN (Figure 3) indicate significant concentrations of PAN in the low stratosphere, evidence for an incursion of polluted air into the lowermost stratosphere. Figure 6 shows scatterplots of observed and simulated HNO3 versus O3 for points above 500 mbar, colored by the TPN mixing ratio. Highest PAN values are associated with the Alaskan fires (18 July) and with the aged tropospheric pollution (2 August). The marked range of TPN values on the stratospheric branches of the scatterplots [from under 100 to above 400 ppt] are a further indication of sporadic exchange and mixing between polluted tropospheric and stratospheric air. These observations caution us that the collocation of high O3 with high PAN does not necessarily indicate that the high O3 was photochemically produced. RAQMS generally represents the pollution and stratospheric branches in HNO3 versus O3 on 18 July, but does not capture the full range of TPN values on each branch. On 2 August RAQMS shows the stratospheric branch in HNO3 versus O3 space, but underestimates the high TPN and HNO3 associated with the tropospheric pollution branch. In addition, RAQMS underestimates highest values of O3 and HNO3 associated with

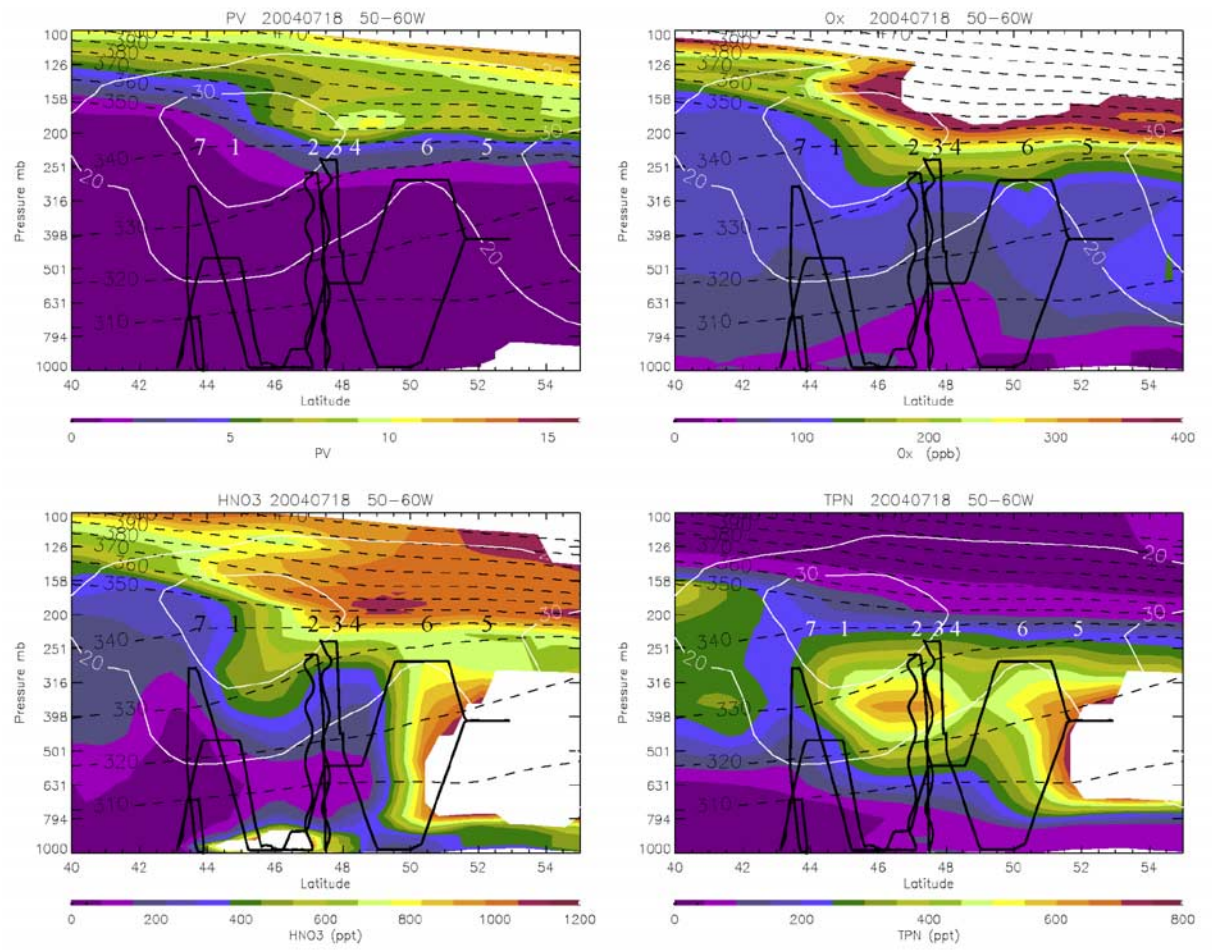

Figure 5a. Cross sections of RAQMS PV, O3, HNO3, and TPN at 1800 UT on 18 July taken along the line marked A–B in Figure 4. Isotachs (white) and isentropes (black dashed) are also shown. The flight altitude profile is projected on to the section (black) Upper level FLs are marked. The A–B section crosses the flight track near FL 3.

the incursion into the lowermost stratosphere, and the range of TPN values observed there. Underestimates of HNO3 and TPN values in the upper troposphere are consistent with weak convective or lightning NOx sources in the model [*Pierce et al.*, 2007]. The model's limited vertical (~200–1000 m) and horizontal resolution near the tropopause likely explains the model's inability to fully capture tracer gradients near the tropopause and to represent the cross-tropopause transport processes responsible for enhanced tracer variability in the lowermost stratosphere.

4. Impact of Large-Scale Deformation: Filamentation Due to Rossby Wave Breaking

[24] In comparing the flights of 18 July and 2 August, we stressed that the flight legs that show highest levels of small-scale ozone variability occurred beneath a depressed tropopause on the poleward side of the jet. One mechanism that could contribute to the observed ozone variability on these flight legs is the quasi-isentropic deformation (folding) of the tropopause and differential advection (shear strain) in regions of jet acceleration and upper level Rossby wave development [*Thorncroft et al.*, 1993]. Rossby wave amplification can locally enhance PV, temperature, and constituent gradients at the tropopause, can lead to the development of cutoff lows and highs, and at smaller scales the interweaving of tropospheric and stratospheric air in long streamers or filaments [*Appenzeller et al.*, 1996; *Holton et al.*, 1995].

[25] To explore the contribution of large-scale deformation to the tracer variability observed from the DC8 on the upper level flight legs, we conducted back trajectory simulations and applied a trajectory mapping technique to RAQMS analyses of the DC8 flight curtain (Figure 3) and to selected horizontal surfaces. Back trajectories were conducted using the LaRC trajectory model (LTM) using the 3-D wind fields of the RAQMS model. Chemical and dynamical fields from RAQMS were sampled along the trajectory paths, and Lagrangian averages of these fields were mapped to the initial parcel locations. This variation on the RDF method [*Sutton et al.*, 1994] is intended to provide information about time-averaged air parcel history and to represent tracer variability which can be attributed to

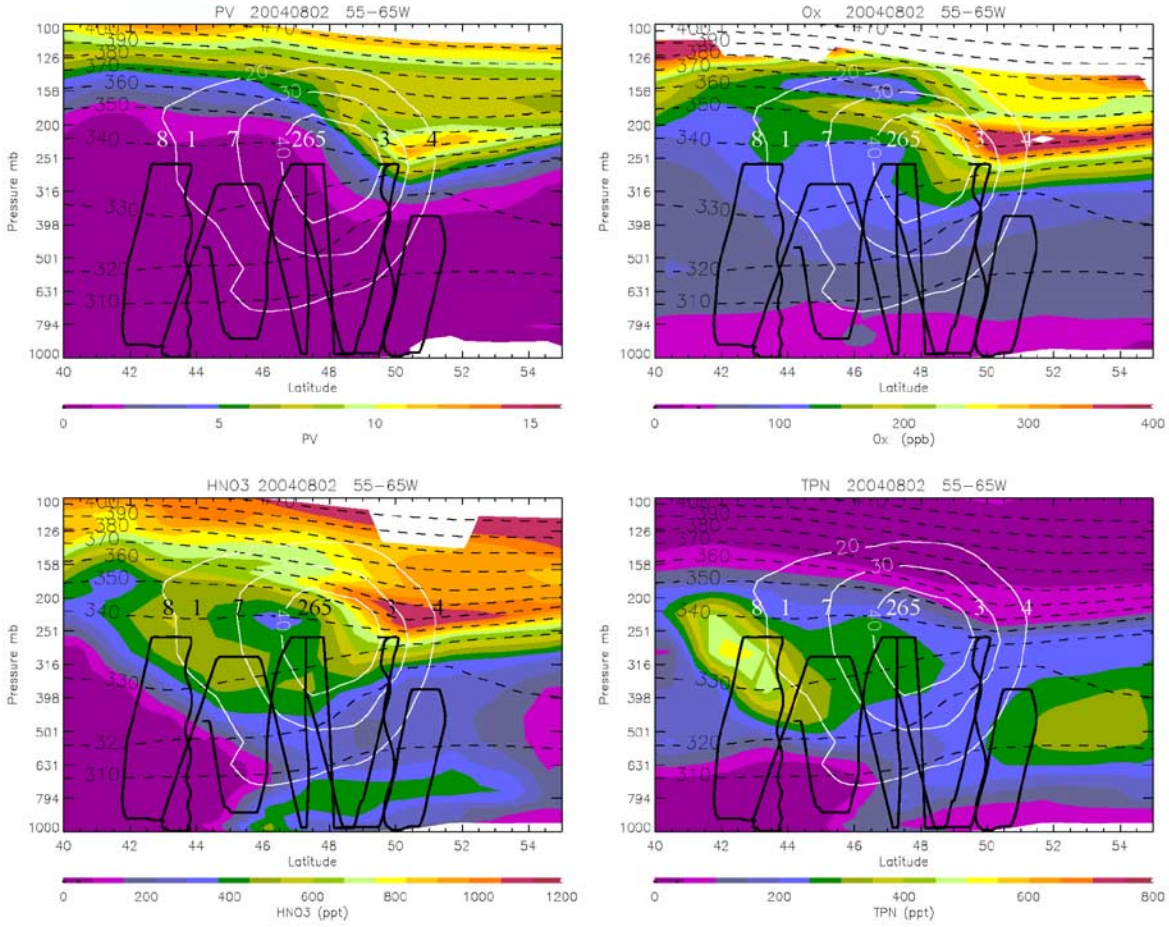

Figure 5b. As for Figure 5a but cross sections are along line C–D in Figure 4 for 2 August.

large-scale deformation, on scales smaller than those that can be represented in conventional analyses. The premise of RDF is that it simulates the nonlinear generation of small-scale tracer variability resulting from differential advection in the large-scale flow [*Sutton et al.*, 1994; *Waugh and Plumb*, 1994], and that this can explain a significant fraction of the observed tracer variability. A similar premise applies to the contour advection technique [*Norton*, 1994; *Waugh and Plumb*, 1994]. For analysis of the flight curtains, air parcels were initialized at 1-min intervals on RAQMS vertical grid; for mapped RDF products, parcels were initialized on a uniform grid of 0.5° by 0.5°. The RDF products shown here are 2-day Lagrangian averages of selected quantities sampled at 2-hour intervals along the back trajectories. For trajectory lengths longer than 2 days, the Lagrangian averages show reduced correlation and higher RMS differences compared with the observed data, which we attribute to accumulated errors in the advection, and breakdown in air parcel integrity along a trajectory path [*Sutton et al.*, 1994; *Beuermann et al.*, 2002].

[26] Figure 7 shows 2-day RDF O3 along the flight curtain for 1800 UT on 18 July with the DC8 flight profile superimposed. A time series of the in situ ozone is also shown, together with the analyzed and RDF time series from RAQMS. Figure 7 (top) may be compared with those shown in Figure 2. Figure 7 (bottom) shows local expansions of the time series plot for time periods encompassing FLs 3 and 7 respectively. The RDF time series adds some information about the time evolution of ozone on FL3, notably a single wave-like oscillation along the flight leg, that is discernable in the data but not so in the RAQMS analysis. In addition, the RDF series is better correlated (r = 0.73) than the analyzed series (r = 0.52) and mean-bias-adjusted RMS difference is reduced (20 ppb versus 26 ppb) compared with 1-min averaged in situ ozone data for FL3. On the other hand RDF shows a higher bias for FL3 versus observations (91 ppb versus 34 ppb), associated with descent of high ozone on the poleward side of the jet. A 20% high bias in RAQMS O3 between 100 and 300 mbar [*Pierce et al.*, 2007] likely contributes to this bias, but too strong descent cannot be discounted. For FL7, which occurs well beneath the strong O3 gradients at the tropopause, and shows little observed variability, RDF is successful in introducing no additional mesoscale structure compared with the model analysis. (The mean-bias-adjusted RMS difference was reduced from 7.3 ppb to 6.7 ppb, and the correlation coefficient increased from r = 0.15 to 0.43, but the mean bias increased from 4.0 ppb to 7.0 ppb.) On either FL the 2-day RDF provides no information about ozone variability at scales smaller than about 10 min,

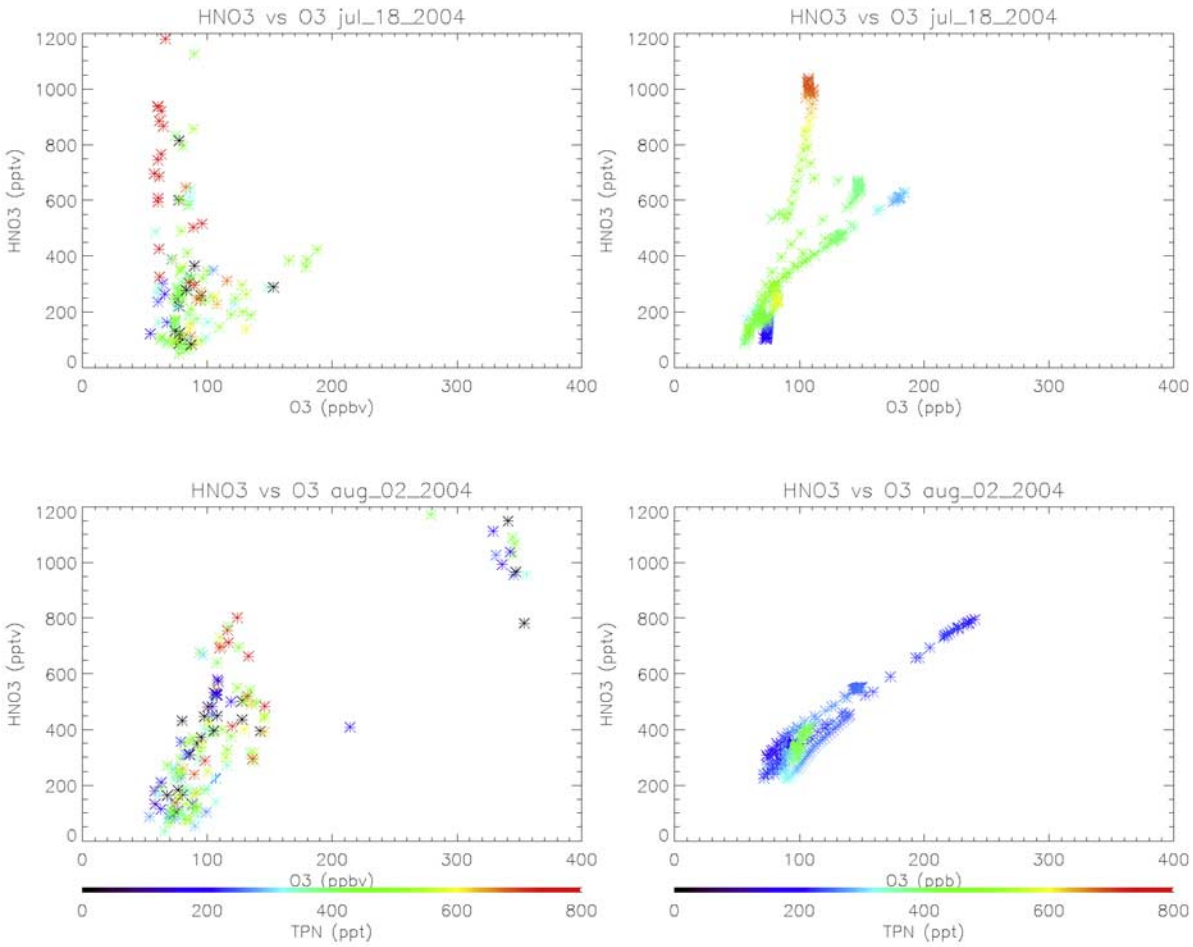

Figure 6. Scatterplots of (left) in situ and(right) simulated HNO3 versus O3 for (top) 18 July and (bottom) 2 August for data points located above 500 mbar. The points are colored by observed and simulated TPN mixing ratio, respectively. The observational data are taken at the frequency of the HNO3 measurements.

suggesting that processes other than large-scale deformation are responsible.

[27] Figure 8 shows maps of 2-day RDF ozone, Lagrangian pressure change (Δp) and RDF Q at 330 K for 1800 UT on 18 July (see Figure 8 caption for details). The Lagrangian Δp map shows the vertical displacement of parcels in the previous 2 days ($\Delta p > 0$ (<0) corresponds to descent (ascent)). The RDF O3 map may be compared with the corresponding analysis shown in Figure 4. The map shows a narrow filament of high ozone crossing the flight track just east of FL3 on the western flank of the jet, composed of parcels that have descended strongly in the previous 2 days. The elongated structure is consistent with upstream descent and cross-jet differential advection, characteristic of upper level frontogenesis [*Shapiro*, 1981]. Parallel to the ozone streamer on the eastern side of the jet are parcels ascending in a warm conveyor belt, associated with the cyclonic development ($\Delta p < -100$ mbar day^{-1}). The RDF map also shows a number of refinements of features in the ozone analysis in Figure 4. Notably, the streamer of elevated ozone stretched across the DC8 flight track near FL3 is shown to be a refinement of a high ozone anomaly in Figure 4. This streamer appears as an O3 maximum in latter half of FL3 (Figure 7) and shows up on the flight curtain as a narrow fold of high ozone extending downward on the poleward side of the jet. The map of Δp confirms that this feature arises from descent (see above discussion). In addition, the RDF map indicates the high ozone air mass enclosed in the deep upper level trough joined to stratospheric air on the polar side of the polar jet near 60°N, which the DC8 sampled near FL6 at 1915 UT. The ozone structure within the upper trough fits the pattern of a Type II (cyclonic) intrusion and rollup of stratospheric influenced air into the upper troposphere [*Appenzeller et al.*, 1996]. The western flank of the upper level trough (eastern flank of the upstream ridge) is a preferred region for adiabatic descent and folding of the tropopause and for Rossby wave breaking [*Holton et al.*, 1995; *Appenzeller et al.*, 1996; *Postel and Hitchman*, 1999].

[28] We use RDF Q to distinguish air masses that have experienced significant horizontal shear strain deformation over the previous 2 days from those that have stayed under more coherent, rotational conditions. The RDF map of Q for 18 July in Figure 8 shows negative values characteristic of

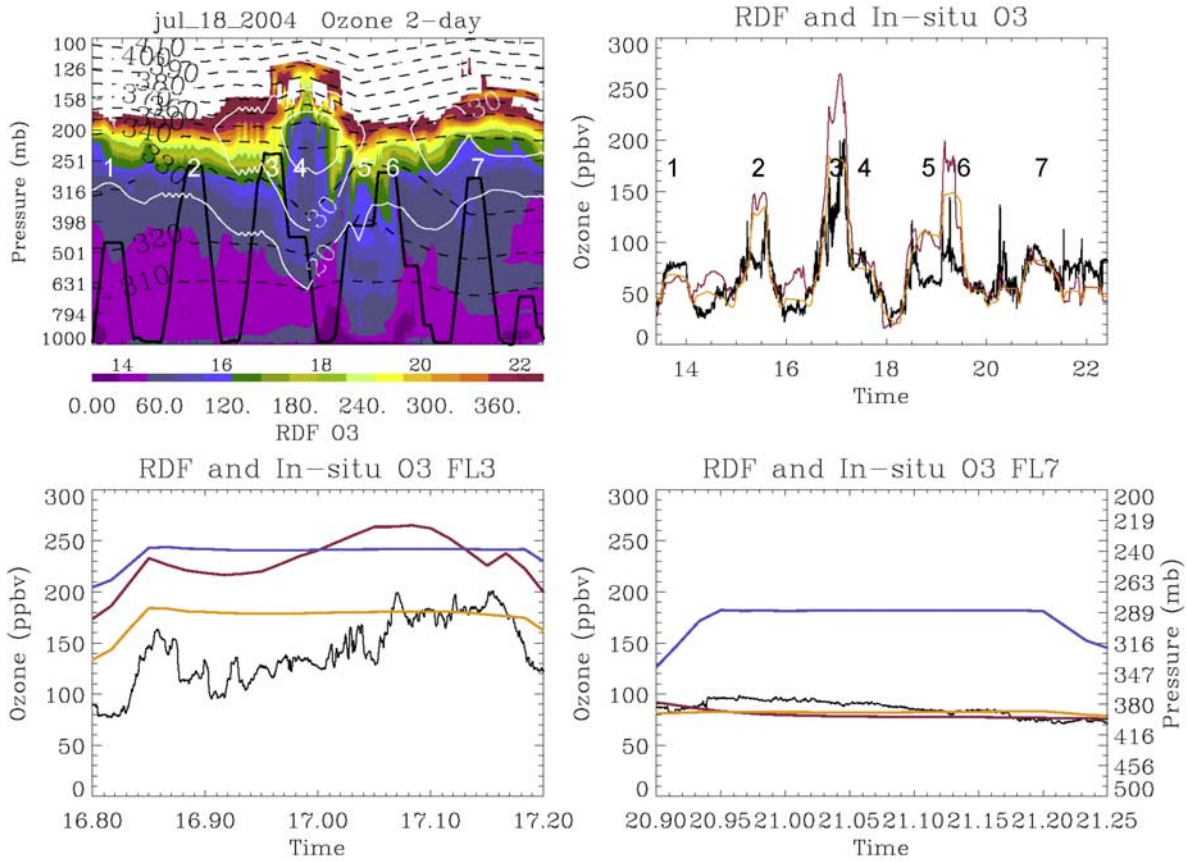

Figure 7. (top left) Two-day RDF ozone along the flight curtain from RAQMS for 18 July. Potential temperature contours (black dashed) and isotachs (white) are also shown, together with the flight altitude (black). (top right) Time series of 1-s in situ ozone (black) together with RAQMS analyzed (yellow) and 2-day RDF (red) ozone. Time series as above but focused on FLs (bottom left) 3 and (bottom right) 7. Pressure at flight altitude is also shown (blue) with axis marked at right (mbar).

rotational flow for air parcels within the upper trough and in the high-pressure system southeast of the flight track. Large, positive values characteristic of shear strain deformation are found on the outer flanks of the trough, the upstream ridge, and the offshore anticyclone and in regions of strong shear associated with the polar and subtropical jets. Notice that the streamers of high O3 in the vicinity of the flight track are closely aligned with high values of Q, consistent with a shear-driven origin for these streamers. Although RDF Q is also positive near FL7, there is little impact on ozone variability since FL7 is far removed from strong ozone gradients near the tropopause and there is no evidence on FL7 of stratospheric influence. In addition, RAQMS indicates that air parcels in the vicinity of FL7 experienced convection in the upper trough in the previous 48 hours. The chemical signatures measured from the DC8 (section 3) are consistent with "aged convection" blending into the upper tropospheric "background," a significant influence on the composition of the upper troposphere during INTEX-NA [*Bertram et al.*, 2007].

[29] Figure 9 shows RDF ozone for the flight curtain on 2 August, together with observed and simulated ozone time series, and expanded time series focused on FLs 3 and 6 for that day. The main impact of RDF on FL3 is to show a more pronounced impact of descent of high O3 values on the poleward side of the jet (compare with Figure 3b), thereby reducing the mean negative bias, from 121 ppb to 51 ppb, between modeled and observed O3. RDF shows no significant improvement in terms of ozone variability over the RAQMS analysis for this FL (the mean-bias-adjusted RMS difference is reduced from 22 ppb to 20 ppb, but the correlation is reduced from r = 0.42 to 0.32) compared with 1-min-averaged in situ ozone data. The RDF maps of ozone and Δp (not shown) confirm strong localized descent of higher ozone on the poleward flank of the jet in the region sampled by FL3, but little additional refinement of structure over the analyzed map of O3 (Figure 4). For FL6, which showed little observed O3 variability, RDF showed insignificant change in mean-bias-adjusted RMS difference, although a 10% negative bias was introduced.

5. Origin of Smaller-Scale Variability

[30] The above examination indicates that filamentation associated with descent and differential advection on the poleward side of the jet can explain some of the larger-scale features encountered on level flight legs on 18 July.

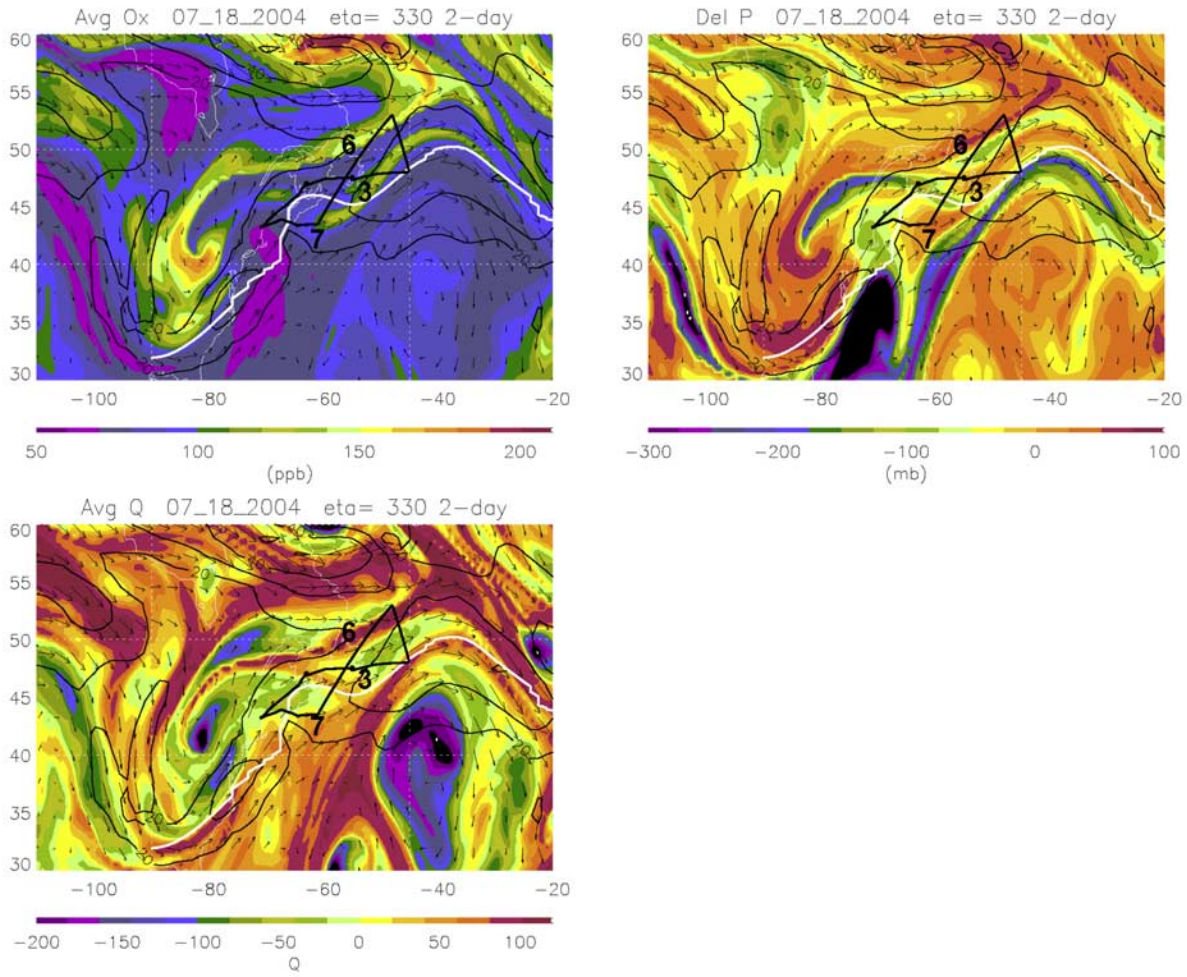

Figure 8. Two-day RDF maps of ozone, and Q at 330 K, with a 2-day map of Lagrangian Δp for 1800 UT on 18 July. For the Q field, what is actually shown is the signed square-root of Q (see section 2.4); units are m s^{-1}. Isotachs (black contours), wind arrows, and the flight track on 18 July (black) with selected FLs are also shown. White lines mark the axis of strongest winds on the 330 K surface in each map.

However, the in situ data shown in Figure 7 indicate significant energy at finer scales in the O3 time series. *Danielsen et al.* [1991] and *Chan et al.* [1991] examined tracer and dynamical structure in the vicinity of the subtropical jet during the 1984 STEP campaign. Chan et al. found evidence for a vertically propagating elliptically polarized inertio-gravity wave in the low stratosphere, while Danielsen et al. illustrated the perturbation of tracer gradients by such a wave, and diagnosed the existence of higher-frequency buoyancy waves whose breaking can lead to irreversible mixing across tracer gradients. *Holton* [1987] argued that tracer variability arising from Rossby wave activity is not correlated with potential temperature, θ, whereas buoyancy-wave-induced tracer variability is correlated with θ. Here we examine how ozone variability observed on 18 July is related to temperature and wind perturbations and assess the extent to which wave motions can account for the observed small-scale ozone structures.

[31] To conduct this analysis we took the 1-s time series of O3, potential temperature (θ), u and v velocity components on FL3 and constructed 10-s average data, in order to account for the lower sampling frequency for temperature measurements on the DC8. We followed the approach of *Teitelbaum et al.* [1996] in examining the correlation of O3 and θ residual perturbations as follows: We remove linear trends from the 10-s data and apply a "medium pass filter," eliminating oscillations with periods less than 250 s ($\sim$50 km of level flight). This limit was suggested by a local minimum in the power spectrum for O3 along FL3. High-frequency residuals of O3 and θ were obtained as normalized differences between the smoothed data and the 10-s data. We scaled the θ residuals by the ratio of the normalized spatial derivatives of smoothed O3 to smoothed θ along FL3 to account for differences in the medium-scale gradients of O3 and θ [*Pierce and Grant*, 1998].

[32] Figure 10 shows the results of this procedure for O3 and θ. We recall that on FL3 the DC8 approaches the jet core from the west. Figures 10a and 10b show 10-s O3 and θ respectively on FL3, together with linear trends (dashed), and medium-pass-filtered data (dotted). The normalized residuals of O3 and θ are shown in Figure 10c, together with a running profile of the cross-correlation coefficient,

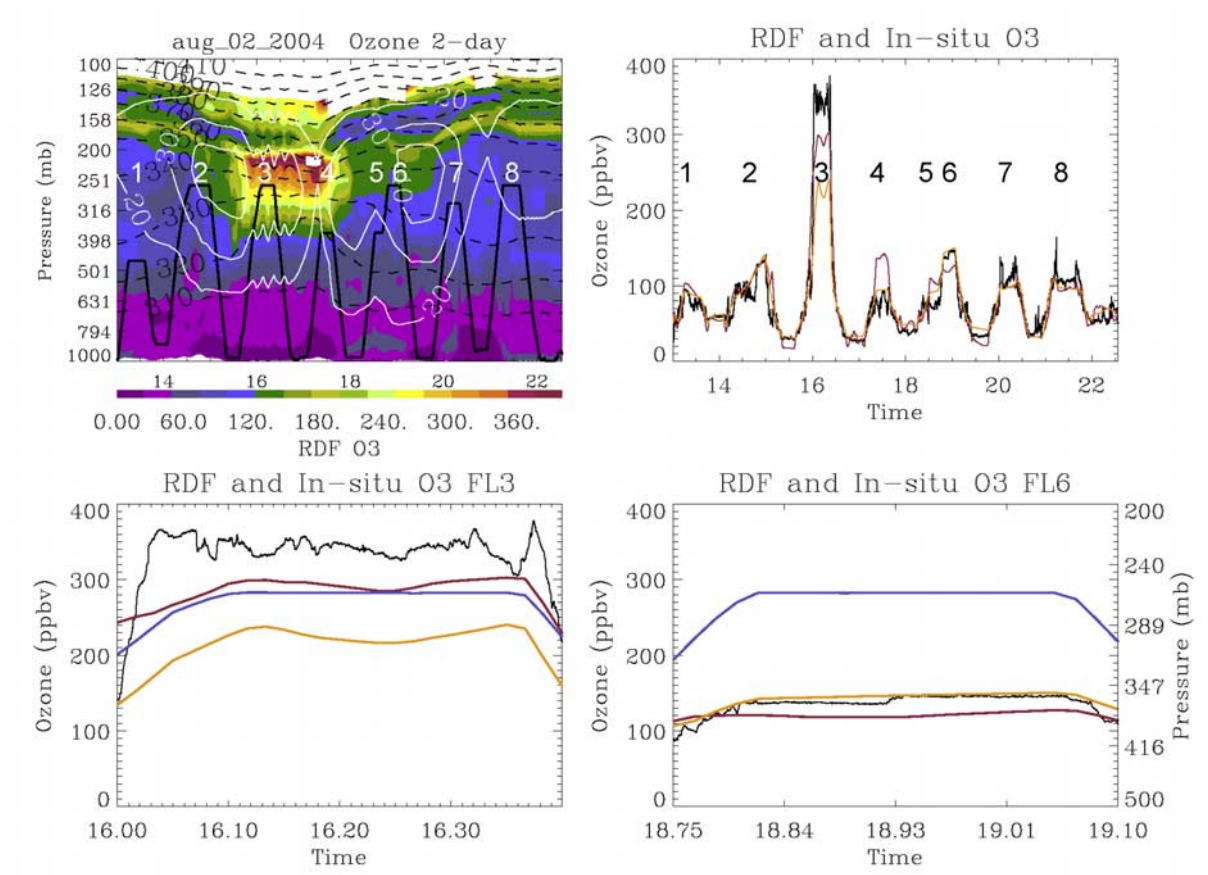

Figure 9. (top left) Two-day RDF ozone along the flight curtain from RAQMS for 2 August. Potential temperature contours (black dashed) and isotachs (white) are also shown, together with the flight altitude (black). (top right) Time series of 1-s in situ ozone (black) together with RAQMS analyzed (yellow) and 2-day RDF (red) ozone. Time series as above but focused on FLs (bottom left) 3 and (bottom right) 6. Pressure at flight altitude is also shown (blue) with axis marked at right (mbar).

evaluated in 5-min intervals. The residuals show significant energy for timescales in the range 30 s to 120 s (~6 to 24 km). The O3 and θ residuals are highly correlated in the middle section of the flight leg, consistent with buoyancy wave oscillations [*Pierce and Grant*, 1998]. Like the O3 and θ residuals the u and v residuals (not shown) show considerable energy at 24 km scales and below. There is little doubt that the oscillations shown by the residual profiles in Figure 10 reflect gravity wave oscillations. Turbulence associated with breaking gravity waves can lead to efficient mixing across air mass boundaries [*Danielsen et al.*, 1991] and could explain the mixing signatures found in tracer-tracer correlation plots.

6. Conclusions

[33] In this paper we have used in situ observations taken from 2 DC8 flights during INTEX-NA to study the characteristics of small-scale tracer structure in the upper troposphere in the vicinity of the subtropical jet. Both flights took place over a similar geographic domain, yet one showed a high degree of small-scale tracer variability on level flight legs, whereas the other did not. When viewed in a reference frame relative to the subtropical jet, the differences became clear. Small-scale tracer structure was particularly pronounced on level flight legs, poleward of the jet core and just beneath the strong tracer gradients defining the tropopause; in contrast such structure was much weaker under an elevated tropopause, equatorward of the jet. Coincident with enhanced small-scale variability, in situ observations on 18 July showed evidence for interleaving and mixing of stratospheric and polluted tropospheric air in the upper troposphere. On the flight of 2 August, the DC8 sampled the low stratosphere on the poleward side of the jet, where evidence for an intrusion of polluted air from the troposphere was found. On the same day, more aged pollution was found in the upper troposphere on the tropical side of the jet. We used trajectory mapping (RDF) of 3-D model (RAQMS) chemical and dynamical fields to demonstrate that filamentary structure, generated via descent and differential advection on the poleward side of the jet, contributed to the subgrid-scale variability observed in the upper troposphere on 18 July. For the case considered here RDF showed skill in refining tracer structure seen in RAQMS analyzed fields. In addition, filamentary O3 structure was found closely aligned with high positive values of Lagrangian-averaged Q, a measure used to distinguish air masses that have experienced enhanced shear strain deformation

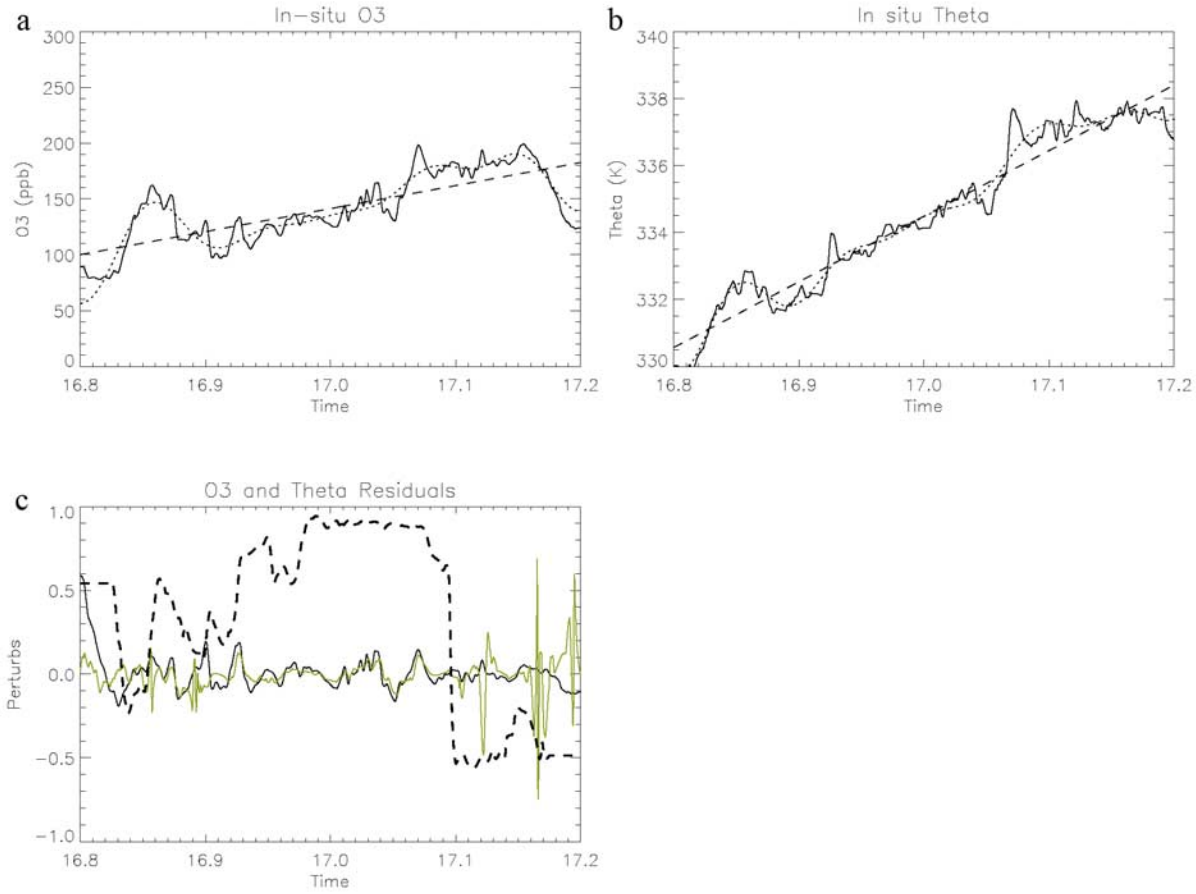

Figure 10. Analysis of in situ O3, and potential temperature, θ, for FL3 on 18 July: time series of 10-s (a) O3 and (b) θ (black solid), together with linear trends (dashed), and medium-pass-filtered data (dotted). (c) Normalized residuals of O3 (black) and θ (green) data with medium-pass-filtered data removed. The θ residuals are multiplied by a scaling factor (see text for details). Also shown is the correlation between the residuals (black dashed).

from those subject to more stable rotational conditions. It remains to be seen whether RDF and Q show statistically significant skill in predicting shear-driven, high-frequency tracer variability in the vicinity of upper tropospheric jet streams.

[34] Higher-frequency tracer and dynamical structures observed on 18 July were found to be characteristic of gravity wave oscillations. Turbulence associated with breaking gravity waves is known to be an efficient vehicle for mixing across tracer gradients. The observation of mixed polluted and stratospheric air mass signatures colocated with gravity wave activity in the upper troposphere on the poleward side of the jet suggests that gravity wave turbulence was responsible for the irreversible mixing of air in the vicinity of the tropopause.

[35] In this study, we do not attempt to quantify the degree of stratospheric exchange with the upper troposphere during INTEX-NA, but simply to illuminate some of the mechanisms responsible for observed structure along upper level flight tracks. *Thompson et al.* [2007] used ozonesonde data to estimate that 35% of tropospheric O3 was stratospherically influenced in the INTEX domain. In contrast, *Fuelberg et al.* [2007] found that 27% of air parcel trajectories from DC8 flight tracks encountered the stratosphere within the previous 10 days. This study suggests that the extent of small-scale variability and the degree of mixing across the troposphere was larger than 3-D models estimate. As we rely more and more on remotely sensed measurements from satellite to monitor atmospheric composition, understanding the full extent of tracer variability in the vicinity of jet streams in the upper troposphere/lower stratosphere is important not only for validating current satellite measurements [*Sparling et al.*, 2006], but for designing the suite of instruments to come.

[36] **Acknowledgments.** The authors wish to thank J. Plant (NASA LaRC), R. Cohen, A. Perring, P. J. Wooldridge and T. Bertram (U.C. Berkeley) for their contribution of measurements and discussions; L. Pfister (NASA ARC) for very helpful discussions; and helpful comments and suggestions of three anonymous reviewers. This work was funded by the NASA Science Mission Directorate, Atmospheric Composition program.

References

Al-Saadi, J. A., et al. (2005), Improving national air quality forecasts with satellite aerosol observations, *Bull. Am. Meteorol. Soc.*, *86*(9), 1249–1261.

Appenzeller, C., H. C. Davies, and W. A. Norton (1996), Fragmentation of stratospheric intrusions, *J. Geophys. Res.*, *101*(D1), 1435–1456.

Aref, H., and S. Balachander (1986), Chaotic advection in Stokes flow, *Phys. Fluids*, *29*(11), 3515–3521.

Avery, M. A., D. J. Westberg, H. E. Fuelberg, R. E. Newell, B. E. Anderson, S. A. Vay, G. W. Sachse, and D. R. Blake (2001), Chemical transport across the ITCZ in the central Pacific during an ENSO cold phase event in March/April of 1999, *J. Geophys. Res.*, *106*, 32,539–32,554.

Bertram, T. H., et al. (2007), Direct measurements of the convective recycling of the upper troposphere, *Science*, *315*(5813), 816–820, doi:10.1126/science.1134548.

Beuermann, J., et al. (2002), High resolution measurements of stratospheric and tropospheric intrusions in the vicinity of the polar jet stream, *Geophys. Res. Lett.*, *29*(12), 1577, doi:10.1029/2001GL014162.

Chameides, W., and D. Davis (1982), Chemistry of the troposphere, *Chem. Eng. News*, *60*(40), 38–52.

Chan, K. R., S. G. Scott, S. W. Bowen, S. E. Ganies, E. F. Danielsen, and L. Pfister (1991), Horizontal wind fluctuations in the stratosphere during large-scale cyclogenesis, *J. Geophys. Res.*, *96*(D9), 17,425–17,432.

Cho, J. Y. N., et al. (1999), Observations of convective and dynamical instabilities in tropopause folds and their contribution to stratosphere-troposphere exchange, *J. Geophys. Res.*, *104*(D17), 21,549–21,568.

Cooper, O. R., et al. (2004), A case study of transpacific warm conveyor belt transport: Influence of merging airstreams on trace gas import to North America, *J. Geophys. Res.*, *109*, D23S08, doi:10.1029/2003JD003624.

Danielsen, E. F., et al. (1991), Irreversible transport in the stratosphere by internal waves of short vertical wavelength, *J. Geophys. Res.*, *96*(D9), 17,433–17,452.

Dibb, J. E., E. Scheuer, M. Avery, J. Plant, and G. Sachse (2006), In situ evidence for renitrification in the Arctic lower stratosphere during the polar aura validation experiment (PAVE), *Geophys. Res. Lett.*, *33*, L12815, doi:10.1029/2006GL026243.

Esler, J. G., P. H. Haynes, K. S. Law, H. Barjat, K. Dewey, J. Kent, S. Schmitgen, and N. Brough (2003), Transport and mixing between air masses in cold frontal regions during Dynamics and Chemistry of Frontal Zones (DCFZ), *J. Geophys. Res.*, *108*(D4), 4142, doi:10.1029/2001JD001494.

Fairlie, T. D., R. B. Pierce, W. L. Grose, G. Lingenfelser, M. Loewenstein, and J. R. Podolske (1997), Lagrangian forecasting during ASHOE/MAESA: Analysis of predictive skill for analyzed and reverse-domain-filled potential vorticity, *J. Geophys. Res.*, *102*(D11), 13,169–13,182.

Fairlie, T. D., M. H. Proffitt, and C. R. Webster (1999), The contribution of mixing in Lagrangian photochemical predictions of polar ozone loss over the Arctic in summer 1997, *J. Geophys. Res.*, *104*(D21), 26,597–26,610.

Fehsenfeld, F. C., et al. (2006), International Consortium for Atmospheric Research on Transport and Transformation (ICARTT): North America to Europe—Overview of the 2004 summer field study, *J. Geophys. Res.*, *111*, D23S01, doi:10.1029/2006JD007829.

Fishman, J., and P. Crutzen (1978), The origin of ozone in the troposphere, *Nature*, *274*, 855–858.

Fishman, J., V. Ramanathan, P. J. Crutzen, and S. C. Liu (1979), Tropospheric ozone and climate, *Nature*, *282*, 818–820.

Forster, P. M. de. F., and K. P. Shine (1997), Radiative forcing and temperature trends from stratospheric ozone changes, *J. Geophys. Res.*, *102*(D9), 10,841–10,856.

Fuelberg, H. E., M. J. Porter, C. M. Kiley, J. J. Halland, and D. Morse (2007), Meteorological conditions and anomalies during the Intercontinental Chemical Transport Experiment–North America, *J. Geophys. Res.*, *112*, D12S06, doi:10.1029/2006JD007734.

Goldstein, A. H., et al. (2004), Impact of Asian emissions on observations at Trinidad Head, California, during ITCT 2K2, *J. Geophys. Res.*, *109*, D23S17, doi:10.1029/2003JD004406.

Haynes, P. H. (1990), High-resolution three-dimensional modeling of stratospheric flows: Quasi-two-dimensional turbulence dominated by a single vortex, in *Topological Fluid Mechanics*, edited by H. K. Moffatt and A. Tsinober, pp. 345–354, Cambridge Univ. Press, New York.

Holton, J. R. (1987), The production of temporal variability in trace constituent correlations, in *Transport Processes in the Atmosphere*, edited by G. Visconti and R. Garcia, pp. 313–326, Springer, New York.

Holton, J. R., P. H. Haynes, M. E. McIntyre, A. R. Douglass, R. B. Rood, and L. Pfister (1995), Stratosphere-troposphere exchange, *Rev. Geophys.*, *33*(4), 403–440.

Hov, O., et al. (1984), Organic gases in the Norwegian Arctic, *Geophys. Res. Lett.*, *11*(5), 425–428.

Jacob, D. J., and A. Gilliland (2005), Modeling the impact of air pollution on global climate change, *Environ. Manager.*, 24–26.

Kim, S., et al. (2007), Measurement of HO_2NO_2 in the free troposphere during the Intercontinental Chemical Transport Experiment–North America 2004, *J. Geophys. Res.*, *112*, D12S01, doi:10.1029/2006JD007676.

Liu, S. C., D. Kley, M. McFarland, J. D. Mahlman, and H. Levy II (1980), On the origin of tropospheric ozone, *J. Geophys. Res.*, *85*, 7546–7552.

Logan, J. A. (1985), Tropospheric ozone—Seasonal behavior, trends, and anthropogenic influence, *J. Geophys. Res.*, *90*, 10,463–10,482.

Logan, J. A., M. J. Prather, S. C. Wofsy, and M. B. McElroy (1981), Tropospheric chemistry: A global perspective, *J. Geophys. Res.*, *86*, 7210–7254.

Murphy, D. M. (1989), Time offsets and power spectra of the ER-2 data set from the 1987 Airborne Antarctic Ozone Experiment, *J. Geophys. Res.*, *94*(D14), 16,737–16,748.

Norton, W. A. (1994), Breaking Rossby waves in a model stratosphere diagnosed by a vortex-following coordinate system and a technique for advecting material contours, *J. Atmos. Sci.*, *51*(4), 654–673.

Ottino, J. M. (1989), *The Kinematics of Mixing: Stretching, Chaos, and Transport*, 364 pp., Cambridge Univ. Press, New York.

Pierce, R. B., and T. D. Fairlie (1993), Chaotic advection in the stratosphere: Implications for the dispersal of chemically perturbed air from the polar vortex, *J. Geophys. Res.*, *98*(D10), 18,589–18,595.

Pierce, R. B., and W. B. Grant (1998), Seasonal evolution of Rossby and gravity wave induced laminae in ozonesonde data obtained from Wallops Island, Virginia, *Geophys. Res. Lett.*, *25*(11), 1859–1862.

Pierce, R. B., T. D. Fairlie, W. L. Grose, R. Swinbank, and A. O'Neill (1994), Mixing processes within the Polar Night Jet, *J. Atmos. Sci.*, *51*(20), 2957–2972.

Pierce, R. B., et al. (2002), Large-scale chemical evolution of the Arctic vortex during the 1999/2000 winter: HALOE/POAM III Lagrangian photochemical modeling for the SAGE III—Ozone Loss and Validation Experiment (SOLVE) campaign, *J. Geophys. Res.*, *107*, 8317, doi:10.1029/2001JD001063. [printed *108*(D5), 2003].

Pierce, R. B., et al. (2003), Regional Air Quality Modeling System (RAQMS) predictions of the tropospheric ozone budget over east Asia, *J. Geophys. Res.*, *108*(D21), 8825, doi:10.1029/2002JD003176.

Pierce, R. B., et al. (2007), Chemical data assimilation estimates of continental U.S. ozone and nitrogen budgets during the Intercontinental Chemical Transport Experiment–North America, *J. Geophys. Res.*, *112*, D12S21, doi:10.1029/2006JD007722.

Postel, G. A., and M. H. Hitchman (1999), A climatology of Rossby wave breaking along the subtropical tropopause, *J. Atmos. Sci.*, *56*(3), 359–373.

Sachse, G. W., G. F. Hill, L. O. Wade, and M. G. Perry (1987), Fast-response, high-precision carbon monoxide sensor using a tunable diode laser absorption technique, *J. Geophys. Res.*, *92*, 2071–2081.

Shapiro, M. A. (1980), Turbulent mixing within tropopause folds as a mechanism for the exchange of chemical constituents between the stratosphere and troposphere, *J. Atmos. Sci.*, *37*(5), 994–1004.

Shapiro, M. A. (1981), Frontogenesis and geostrophically forced secondary circulations in the vicinity of jet stream-frontal zone systems, *J. Atmos. Sci.*, *38*(5), 954–973.

Singh, H. B., W. H. Brune, J. H. Crawford, D. J. Jacob, and P. B. Russell (2006), Overview of the summer 2004 Intercontinental Chemical Transport Experiment–North America (INTEX-A), *J. Geophys. Res.*, *111*, D24S01, doi:10.1029/2006JD007905.

Singh, H. B., et al. (2007), Reactive nitrogen distribution and partitioning in the North American troposphere and lowermost stratosphere, *J. Geophys. Res.*, *112*, D12S04, doi:10.1029/2006JD007664.

Sparling, L. C., J. C. Wei, and L. M. Avallone (2006), Estimating the impact of small-scale variability in satellite measurement validation, *J. Geophys. Res.*, *111*, D20310, doi:10.1029/2005JD006943.

Sutton, R. T., H. Maclean, R. Swinbank, A. O'Neill, and F. W. Taylor (1994), High-resolution stratospheric tracer fields estimated from satellite observations using Lagrangian trajectory calculations, *J. Atmos. Sci.*, *51*(20), 2995–3005.

Talukdar, R. K., J. B. Burkholder, A.-M. Schmoltner, J. M. Roberts, R. W. Wilson, and A. R. Ravishankara (1995), Investigation of the loss processes for peroxyacetyl nitrate in the atmosphere: UV photolysis and reaction with OH, *J. Geophys. Res.*, *100*(D7), 14,163–14,174.

Teitelbaum, H., M. Moustaoui, J. Ovarlez, and H. Kelder (1996), The role of atmospheric waves in the laminated structure of ozone profiles at high latitude, *Tellus, Ser. A*, *48*, 442–455.

Thompson, A. M., et al. (2007), Intercontinental Chemical Transport Experiment Ozonesonde Network Study (IONS) 2004: 1. Summertime upper troposphere/lower stratosphere ozone over northeastern North America, *J. Geophys. Res.*, *112*, D12S12, doi:10.1029/2006JD007441.

Thorncroft, C. D., B. J. Hoskins, and M. E. McIntyre (1993), Two paradigms of baroclinic-wave life-cycle behaviour, *Q. J. R. Meteorol. Soc.*, *119*, 17–55.

Thornton, J. A., P. J. Woodbridge, and R. C. Cohen (1999), Atmospheric NO_2: In situ laser-induced fluorescence detection at parts per trillion mixing ratios, *Anal. Chem.*, *72*(3), 523–539, doi:10.1021/ac9908905S0003-2700(99)00890-2.

Tuck, A. F., S. J. Hovde, and T. P. Bui (2004), Scale Invariance in jet streams: ER-2 data around the lower-stratospheric polar night vortex, *Q. J. R. Meteorol. Soc.*, *130*, 2423–2444.

Tuck, A. F., et al. (2005), Molecular velocity distributions and generalized scale invariance in the turbulent atmosphere, *Faraday Disc.*, *130*, 1–13.

Wang, Y., J. A. Logan, and D. J. Jacob (1998), Global simulation of tropospheric O_3-NO_x-hydrocarbon chemistry: 2. Model evaluation and global ozone budget, *J. Geophys. Res.*, *103*(D9), 10,727–10,755.

Waugh, D. W., and R. A. Plumb (1994), Contour advection with surgery: A technique for investigating finescale structure in tracer transport, *J. Atmos. Sci.*, *51*(4), 530–540.

Zapotocny, T. H., D. R. Johnson, F. M. Reames, R. B. Pierce, and B. J. Wolf (1991), Numerical investigations with a hybrid isentropic sigma model. Part II: The inclusion of moist processes, *J. Atmos. Sci.*, *48*(18), 2025–2043.

Zapotocny, T. H., D. R. Johnson, and F. M. Reames (1994), Development and initial test of the University of Wisconsin Global Isentropic-Sigma Model, *Mon. Weather Rev.*, *122*, 2160–2178.

J. Al-Saadi, M. A. Avery, T. D. Fairlie, R. B. Pierce, and G. Sachse, NASA Langley Research Center, Hampton, VA 23681, USA. (t.d.fairlie@larc.nasa.gov)

J. Dibb, College of Engineering and Physical Sciences, University of New Hampshire, Durham, NH 03824, USA.